Engineering Science and Technology, an International Journal 45 (2023) 101472

HOSTED BY

Contents lists available at ScienceDirect

Engineering Science and Technology, an International Journal

journal homepage: www.elsevier.com/locate/jestch

Maximum power tracking for wind energy conversion systems via a high-order optimal disturbance observer-based LQR without a wind speed sensor

Altynay Kashaganova [a], Kanat Suleimenov [b], Saule Sagnaeva [a], Ton Duc Do [b,*]

[a] Department of System Analysis and Control, Faculty of Information Technology L.N. Gumilyov Eurasian National University, Astana Z01A3D7, Kazakhstan
[b] Department of Robotics and Mechatronics, School of Engineering and Digital Sciences (SEDS), Nazarbayev University, Astana Z05H0P9, Kazakhstan

ARTICLE INFO

Article history:
Received 2 December 2022
Revised 12 June 2023
Accepted 18 June 2023
Available online 13 July 2023

Keywords:
High-order optimal disturbance observer (HOODO)
Linear-quadratic regulator (LQR)
Optimal control
Permanent magnet synchronous generator (PMSG)
Wind energy conversion systems (WECS)

ABSTRACT

A high-order optimal disturbance observer (HOODO) is introduced to precisely estimate the aerodynamic torque and the variable wind speed; and consequently calculate the optimal speed of the generator without measuring the wind speed. As the immeasurable wind speed is varying fast, the aerodynamic torque, which is considered as a disturbance, is also changed fast, then the conventional assumption that the disturbance is slowly-varying (i.e., its first-time derivative is zero), is not applicable. The proposed HOODO design considers the fast and stochastic characteristics of the wind speed by relaxing aforementioned conventional assumption. Moreover, via the linear optimal control theory, the parameters of the HOODO are tuned systematically by proper selection of the elements of the diagonal weighting matrices. In this study, a compromise between the observer's convergence rate and the ability to Gaussian noise suppression is also considered. This helps to solve the difficulties of many existing observers regarding the gain selection algorithms. Also in the article, for the first time, a control scheme is considered in combination with the proposed HOODO and the LQ controller. To maximize a power captured from the wind, a linear-quadratic regulator (LQR) is utilized to maintain the angular speed of the generator at the optimal speed reference. A stability analysis of the designed control scheme is also discussed. Comparative results of the HOODO under different orders as well as other observers are given to prove the effectiveness of the introduced estimation method. The obtained simulation results reveal that the HOODO has a superior estimation of disturbance. All the simulations are carried out in the MATLAB/Simulink software.

1. Introduction

Wind energy is one of the main sources of renewable energy to solve the global warming and pollution associated with fossil fuels. In recent decades, the importance of wind energy has increased significantly among renewable sources [1–5]. Wind energy conversion systems (WECSs) are utilized to generate electric power from the aerodynamic power of the wind. In variable-speed WECSs, the permanent magnet synchronous generator (PMSG) is one of the widely used type of generators [6,7], since it has excellence in terms of high power factor, high power density, high efficiency, and high reliability [8]. However, controlling WECSs is challenging as they have to face with nonlinearities, disturbance, model uncertainty, and modeling errors [9–11] of the system. Moreover, in variable-speed WECSs, the maximum power point tracking (MPPT) problem is essential. With MPPT, the optimum speed reference that the generator has to track is proportional to the wind speed. Anemometers are traditionally used to measure wind speed [12,13]; however, they cannot accurately measure wind speed for control purposes. A feasible solution is to estimate aerodynamic torque and then the wind speed by a disturbance observer (DO) [8,14]. Therefore, a DO-based control system is an effective solution to these issues.

In conventional linear and nonlinear DOs [15–22], a convergence of the estimation error was ensured by considering that a disturbance has slow dynamics with respect to the dynamics of the observer (i.e., the first order time-derivative of a disturbance equals to zero). This kind of assumption is a popular one and works in many practical cases. However, for some particular cases when disturbances have fast dynamics, this assumption is not appropri-

* Corresponding author.
E-mail address: doduc.ton@nu.edu.kz (T.D. Do).
This work was supported by Nazarbayev University under the Faculty Development Competitive Research Grant Program (FDCRGP) with Grant No. 11022021FD2924.

https://doi.org/10.1016/j.jestch.2023.101472
2215-0986/

ate and can lead to unsatisfied estimation performance. The WECS, in which the aerodynamic torque is related to the stochastic wind speed by cubic function relationship, belongs to such type of systems. Shotorbani et al. presented an adaptive nonlinear disturbance observer-based finite time control (FTC) [23]. According to this work, the proposed method has an ability to converge to an equilibrium point in the finite time and it shows better results comparing to the conventional asymptotic convergent controller (ACC). However, during the observer design, an unknown disturbance term is considered as slowly-varying. In the work of Mansouri et al. [24], an optimization of a nonlinear observer using a genetic algorithm is proposed and the speed is estimated by a phase locked loop (PLL). To enhance robustness of the proposed system, a super twisting algorithm is used instead of a traditional PI controller. However, implementation of this method seems complicated since it requires two observers and utilizes a genetic algorithm (GA) which may need additional calculation efforts, consequently make it difficult for hardware implementation. Recently, an optimal control solution to optimal tracking of power in PMSG-based WECS is presented [25]. A sum of squares (SOS) approach was applied to design a nonlinear observer to estimate an aerodynamic torque as well as i_d and i_q currents in WECS. In this proposed method, sum of squares conditions need to be chosen accurately. A nonlinear adaptive control for PMSG-based WECS was proposed in [26]. In this work, a high gain perturbation observer (HGPO) estimates lumped disturbance including nonlinearities, parameter variations, and other external disturbances. Basically, the proposed HGPO is designed based on the Luenberger observer. An improvement for a MPPT control scheme is found in the work of Dali et al. [27]. Although the obtained results of the proposed method show its superiority over traditional methods, detailed analysis about high-order derivatives of disturbances is not presented clearly. A high gain observer is designed for sensorless regulation of a PMSG-based WECS [28]. However, during the observer design, the aerodynamic torque is assumed to be as slowly varying. In another work, active disturbance rejection controller was designed for a WECS [29]. According to this method, the bandwidths of the controller as well as observer are taken as inverses of parameters of internal model controller (IMC) and are replaced by disturbance rejection and setpoint filters. The extended Kalman filter-based optimal controller to estimate and control PMSG-based WECS was presented in the work of Bakhtiari and Nazarzadeh [30]. The designed method shows better performance compared to the conventional PI and linear quadratic Gaussian (LQG). However, additional analysis on fast-changing disturbance conditions should be provided. The extended state observer-based adaptive disturbance rejection control (ADRC) was utiized [31] to estimate disturbances presented in PMSG-based WECS. However, as it is stated in the work of Das et al. [29], when the total disturbance is variable, the ESO cannot guarantee a perfect estimation of disturbance. Moreover, in WECSs with fast parametric changes, unknown external disturbance, and nonlinearities the accurate estimation of disturbance with the ESO is almost impossible. The article of Chen [32] considered a nonlinear disturbance observer-based control (NDOBC). From the presented results, this method is more stable and able to suppress disturbances accurately compared to other robust control methods. Also, the use of a high-order observer shows its robustness to parameter uncertainty, unmodeled errors, and any other type of fast-varying noise [33].

To achieve the desired control system performance, together with conventional proportional-integral-derivative (PID) controllers, many advanced control algorithms for a PMSG exist in the literature. For example, model predictive control (MPC) [34], proportional-integral (PI) control [35], sliding mode control (SMC) [12,36], linear quadratic (LQ) control [33], integral sliding mode control (ISMC) [12,36,37], and neural network based control (NNDC) [38]. A backstepping control [39] was presented to enhance the performance of well-known vector-control (VC) scheme by replacing a traditional PI control widely used in WECS. The backstepping control algorithm shows satisfactory performance under various simulation as well as experimental scenarious, but the comparative results of the presented method with other existing methods is not shown clearly. In another work, a disturbance observer (DOB)-based SMC was utilized to robustly control of a PMSG [12]. Additionally, a fuzzy algorithm was used to switch the gains of the SMC appropriately. Comparing to the fixed-gain SMC, the proposed fuzzy SMC has advantages in terms of chattering reduction, however hardware implementation of this method might be difficult. A linear-quadratic regulator (LQR)-based optimal approach have been introduced by Le and Do [40]. In order to remove nonlinearities and disturbance terms by compensating them in the feedforward loop, the designed control scheme is combined with a high-order disturbance observer. The effectiveness of the presented controller requires a comprehensive analysis by comparing with other existing methods. A model-predictive control (MPC)-based on finite-control-set was designed to overcome the disadvantages existing in a conventional MPC [34]. Although this method shows improved results, its hardware realization needs a real-time setup based on a powerful controller such as field-programmable gate array (FPGA), which in turn adds additional cost to design of overall control system. Disturbance observer-based feedback linearisation control was proposed to improve transient performance under system uncertainty in WECS [35]. This method has a decoupled PI-like design with two extra parts, in which the first part is introduced as an antiwindup compensator, whereas the second part is used to eliminate the effect of sudden step variations in power during the transient period by using the reference jump information. Unfortunately, analysis of the system's performance with the proposed control method under a wind profile with fast dynamics is not shown in the results. Two SMC schemes [36] were presented to control both the mechanical speed of a generator as well as a dc-link voltage. In this work, in order to prove the efficacy of the designed controller over the traditional ones additional comparative studies should be conducted. A research group proposed a novel SMC-based control scheme for a PMSG [41], and the simulation outcomes reveal that with the presented control method a PMSG-based WECS become stable and robust in the region of MPPT. In a recent work [37], a composite controller consisting from a LQR-based ISMC and high-order DO has been presented. In this method, the LQR is designed in the nominal control part, while the ISMC is used to cope with system nonlinearities and parametric uncertainties. The above mentioned control methods greatly improve the control characteristics in various aspects. Although some of these methods are complex and difficult to implement (e.g. NNDC) [38], and for some, under the influence of the mismatched uncertainties, they lose their property as robustness (e.g. SMC) [42].

Considering the previous research works, this paper introduces a high-order optimal DO (HOODO) for estimating aerodynamic torque which, in turn, helps to estimate the wind speed. This paper also utilizes an linear quadratic regulator (LQR), for the speed tracking problem of the generator. The efficiency of the presented optimal composite control scheme is justified by computer simulation in MATLAB/Simulink. The main contribution of this work are: 1) The proposed HOODO relaxes the assumption that disturbance is slowly changed. By doing this, it creates a theoretical base for estimation of fast-varying disturbances such as aerodynamic torque of WECSs precisely; 2) Moreover, to systematically select the gains of the proposed HOODO, an optimal algorithm is utilized. Via tuning the diagonal of weighting matrices, the gains are easily selected for satisfied performance. Note that the gain tuning rule is

a big issue in most of the existing observers; 3) Four different orders of the HOODO, i. e. first, second, third, and fourth order, are compared, analysed and investigated in detail; 4) A straightforward gain tuning rule is implemented for the LQR, which is practical to implement in real hardware; 5) Detailed analysis on stability of the closed-loop HOODO-based LQR is presented explicitly using the Lyapunov approach.

2. Control of a WECS

This section introduces the PMSG-based WECS model [33].

2.1. Wind turbine modelling

The aerodynamic power (P_a) which a wind turbine (WT) can be extracted from the wind is expressed by the following non-linear relationship

$$P_a = \frac{1}{2}\rho\pi R^2 C_p(\lambda,\beta)v^3 \tag{1}$$

where ρ represents the air density, R is the radius of a WT's blade, v is a speed of the wind, $C_p(\lambda,\beta)$ is a WT's power coefficient, which describes the ability of the WT to obtain a mechanical energy from the energy of the wind, λ is a tip-speed ratio (TSR), β represents a pitch angle of the WT's blade.

The power coefficient C_p relates to the TSR λ and blade pitch angle β by nonlinear relationships. The coefficient in most cases are calculated experimentally, hence it is usually reported by the WT's manufacturer. The dependence of the power coefficient $C_p(\lambda,\beta)$ on the TSR λ at a different angle β for a certain blade profile is given in Fig. 1. The figure shows that for each curve, there is one optimal λ, named λ_{opt} at which the power coefficient $C_p(\lambda,\beta)$ reaches its maximum value.

The TSR λ is defined as [43]

$$\lambda = \frac{\omega_t R}{v} \tag{2}$$

where ω_t is the angular speed of the WT's shaft.

Then from (2), the optimal reference angular shaft speed of the WT is determined as

$$\omega_{t,ref} = \frac{\lambda_{opt} v}{R} \tag{3}$$

Here, λ_{opt} is the optimal TSR, at which the power coefficient C_p achieves its maximum value. The ratio in the gearbox of the WT is defined using the following formula,

$$n_{gb} = \frac{\omega}{\omega_t} = \frac{T_a}{T_g} \tag{4}$$

where ω is the generator's angular shaft speed, T_g is a torque of the generator's rotor, T_a is a aerodynamic torque.

On the other hand, the WT's aerodynamic torque depends on the angular speed ω_t through the expression

$$T_a = \frac{P_a}{\omega_t} = \frac{1}{2}\rho\pi R^3 C_q(\lambda,\beta)v^2 \tag{5}$$

where $C_q(\lambda,\beta) = \frac{C_p(\lambda,\beta)}{\lambda}$.

2.2. A model of the PMSG

A structural analysis of the design diagrams of low-power synchronous generators, carried out in [44], showed that multi-pole machines with excitation from permanent magnets outperform other types of generators in terms of efficiency and stability. This is due to the high performance of modern permanent magnets. In this paper, we will consider a PMSG-based WECSs.

We will use the dynamic model of the PMSG as given in [35]:

$$\begin{cases} J\dot{\omega} = -B\omega - T_e + \frac{1}{n_{gb}}T_a \\ \dot{i}_q = -\frac{R_s}{L_s}i_q - P\omega i_d - \frac{\psi_m P}{L_s}\omega + \frac{1}{L_s}u_q + \bar{d}_q \\ \dot{i}_d = -\frac{R_s}{L_s}i_d + P\omega i_q + \frac{1}{L_s}u_d + \bar{d}_d \end{cases} \tag{6}$$

where i_d and i_q are the currents of a generator's stator, u_d and u_q are the voltages in the generator's stator in the direct and quadrature axes, respectively. R_s is a nominal value of the stator's resistance; L_s denotes the nominal value of the stator's inductance; B is a viscous friction coefficient of the shaft of PMSG; ψ_m defines a magnetic flux linkage; J is the inertia of the rotating parts including the wind turbine; P is the pole pairs number; T_a and T_e represent the aerodynamic torque and the electromagnetic torque, respectively. Also, where $\bar{d}_q$ and $\bar{d}_d$ are the terms including parameter uncertainties, noise and modeling errors, which are calculated as follows:

$$\begin{aligned} \bar{d}_q &= \left(\frac{R_s}{L_s} - \frac{R_s+\Delta R_s}{L_s+\Delta L_s}\right)i_q + \left(\frac{\psi_m}{L_s} - \frac{\psi_m+\Delta\psi_m}{L_s+\Delta L_s}\right)P\omega + \left(\frac{1}{L_s} - \frac{1}{L_s+\Delta L_s}\right)u_q + \bar{d}_{qn} \\ \bar{d}_d &= \left(\frac{R_s}{L_s} - \frac{R_s+\Delta R_s}{L_s+\Delta L_s}\right)i_d + \left(\frac{1}{L_s} - \frac{1}{L_s+\Delta L_s}\right)u_d + \bar{d}_{dn} \end{aligned} \tag{7}$$

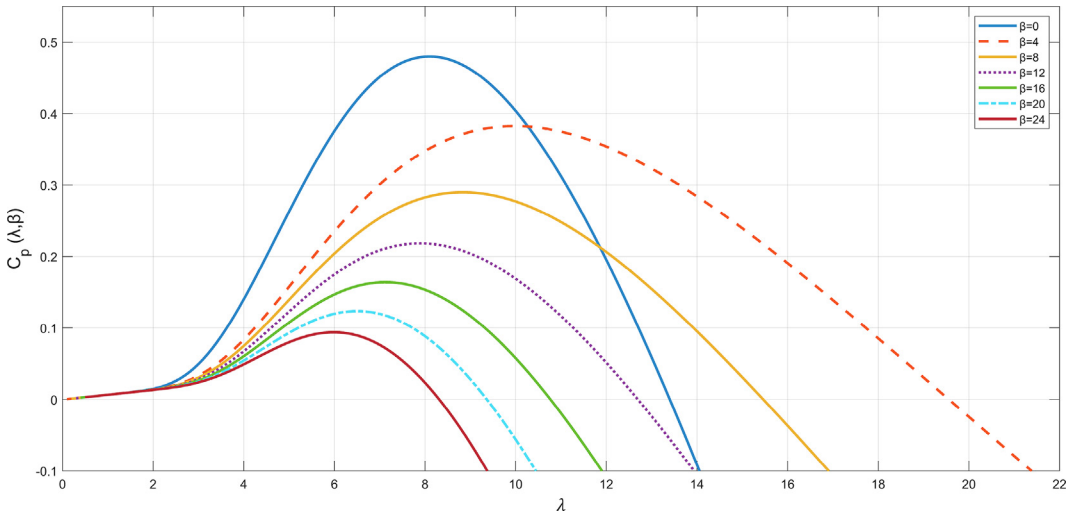

Fig. 1. Relation between C_p and tip speed ratio λ at different value of blade pitch angle β.

where ΔR_s and ΔL_s are the variations of stator resistance and inductance, respectively, $\bar{d}_{qn}$ and $\bar{d}_{dn}$ are the noise and modeling errors.

In the system (6), the electromagnetic torque T_e is determined by the formula:

$$T_e = Ki_q \tag{8}$$

where $K = \frac{3}{2}(\psi_m P)$ is the torque coefficient.

In next sections, the control system design is being carried out under the following assumptions:

Assumption 1: ω, i_d, i_q are available.

Assumption 2: v and T_a are not available.

3. LQR design

The system (6) can be written in terms of an error-based dynamics as below:

$$\begin{cases} \dot{\tilde{\omega}} = -\frac{B}{J}\tilde{\omega} - \frac{1}{JK}\tilde{i}_q \\ \dot{\tilde{i}}_q = -\frac{R_s}{L_s}\tilde{i}_q - \frac{\psi_m P}{L_s}\tilde{\omega} + \frac{1}{L_s}(u_q - u_{ffq}) \\ \dot{i}_d = -\frac{R_s}{L_s} i_d + \frac{1}{L_s}(u_d - u_{ffd}) \end{cases} \tag{9}$$

where $\tilde{\omega}$ is a speed tracking error of the rotor, $\tilde{i}_q$ is the q-axis stator's current tracking error, and u_{ffq} and u_{ffd} are control inputs serving as compensating terms in the feedforward loop. The tracking errors are determined by,

$$\begin{aligned} &\tilde{\omega} = \omega - \omega_{ref}; \omega_{ref} = \omega_{t,ref} \cdot n_{gb} = \tfrac{\lambda_{opt}}{R} v \cdot n_{gb} \\ &\tilde{i}_q = i_q - i_{q_{ref}}; i_{q,ref} = \tfrac{1}{Kn_{gb}} T_a - \tfrac{B}{K}\omega_{ref} - \tfrac{J}{K}\dot{\omega}_{ref} \\ &u_{ffq} = R_s i_{q,ref} + L i_{q_{ref}} + \psi_m P \omega_{ref} + P L_s \omega i_d \\ &u_{ffd} = -P L_s \omega i_q \end{aligned} \tag{10}$$

where $\omega_{ref}, i_{q_{ref}}$ are a reference speed of a generator and a reference of a stator current in the q-axis, respectively.

Applying Eqs. 9,10, the mathematical model in the Eqs. (9) and (10) takes the form:

$$\begin{cases} \dot{\tilde{\omega}} = -\frac{B}{J}\tilde{\omega} - \frac{1}{J}\tilde{T}_e \\ \dot{\tilde{T}}_e = -\frac{R_s}{L_s}\tilde{T}_e - \frac{\psi_m PK}{L_s}\tilde{\omega} + \frac{K}{L_s}(u_q - u_{qc}) \\ \dot{i}_d = -\frac{R_s}{L_s} i_d + \frac{1}{L_s}(u_d - u_{dc}) \end{cases} \tag{11}$$

$$\begin{aligned} &\tilde{T}_e = T_e - T_{e_{ref}}; T_{e_{ref}} = \tfrac{1}{n_{gb}} T_a - B\omega_{ref} - J\dot{\omega}_{ref} \\ &u_{qc} = \tfrac{R_s}{K} T_{e_{ref}} + \tfrac{L_s}{K} \dot{T}_{e_{ref}} + \psi_m P \omega_{ref} + P L_s \omega i_d \\ &u_{dc} = -\tfrac{P L_s}{K} \omega T_e \end{aligned} \tag{12}$$

We note that ω_{ref} and $i_{q_{ref}}$ are unknown, since v and T_a are unknown by Assumption 2. To estimate T_a and v, details on design of the HOODO will be given in the following sections.

The system in (11) can be rewritten in the state-space form as follows,

$$\dot{x} = Ax + B_c(u - u_c) \tag{13}$$

with

$$A = \begin{bmatrix} -\frac{B}{J} & \frac{1}{J} & 0 \\ -\frac{\psi_m PK}{L_s} & -\frac{R_s}{L_s} & 0 \\ 0 & 0 & -\frac{R_s}{L_s} \end{bmatrix}, B_c = \begin{bmatrix} 0 & 0 \\ \frac{K}{L_s} & 0 \\ 0 & \frac{1}{L_s} \end{bmatrix}. \tag{14}$$

where $x = \begin{bmatrix} \tilde{\omega} & \tilde{T}_e & \tilde{i}_d \end{bmatrix}^T, u = [u_q \quad u_d]^T, u_c = [u_{qc} \quad u_{dc}]^T$.

The optimal control law is defined as [45]:

$$u = u_c + K_u x, \tag{15}$$

where $K_u = -R^{-1}B_c^T P_u$ is a calculated gain of the optimal controller, where a positive definite symmetric matrix $P_u > 0$ is a solution of the following algebraic Riccati equation (ARE):

$$P_u A + A^T P_u - P_u B_c R^{-1} B_c^T P_u + Q = 0 \tag{16}$$

with $Q \geqslant 0$ is an 3×3 matrix and $R > 0$ and is a 2×2 matrix. From (15) and (16), it is seen that K_u has dependency on the weight matrices Q and R. Increase of Q positively affects to reference tracking efficiency with more control efforts applied. Increase of R leads to a small control value and poor reference tracking performance. It is recommended to take into account the indicated influence of Q and R on K_u, and to come to a compromise between control efficiency and energy consumption [3]. The weighting matrices are typically chosen as a diagonal ones with non-negative elements on the main diagonal. In this case, however, the presence of some zero values on its main diagonal is allowable.

Theorem 1. The optimal control law in (15) provides an exponential convergence of the state vector x in system (13) to zero.

Proof. Let us define a Lyapunov candidate function $V(x)$ as follows,

$$V(x) = x^T P_u x. \tag{17}$$

Provided that $V(x)$ is radially unbounded positive definite function. Using (13), (15) and (16), the time derivative of $V(x)$ is obtained:

$$\begin{aligned} \dot{V}(x) &= \frac{d}{dt} x^T P_u x = 2x^T P_u (A + B_c K_u) x \\ &= 2x^T P_u \left(A - B_c R^{-1} B_c^T P_u\right) \\ &= x^T P_u \left(P_u A + A^T P_u - 2P_u B_c R^{-1} B_c^T P_u\right) x \leqslant -x^T Q x. \end{aligned} \tag{18}$$

As shown in (18) the first-order time derivative of V is negative for all non-zero x, which, in turn, means that the state vector x exponentially converges to zero. That is, for a given control law (15), the considered system (13) is stable, which was required to be proved.

In the work [46], the deviation of parameters is considered, using ΔA as the value of system parameter variations, the state-dependent coefficient matrix A is rewritten as $A\prime = A + \Delta A$. Therefore, (13) can be rewritten into the following error dynamics:

$$\dot{x} = A\prime x + B_c(u - u_c). \tag{19}$$

The derivative of Lyapunov function in (17) is:

$$\begin{aligned} \dot{V}(x) &= 2x^T P_u \dot{x} \\ &= x^T \left(P_u A + P_u \Delta A + \Delta A^T P_u + A^T P_u - 2P_u B_c R^{-1} B_c^T P_u\right) x \\ &< 0. \end{aligned} \tag{20}$$

Using (16), the derivative becomes

$$\dot{V}(x) = x^T \left(P_u \Delta A + \Delta A^T P_u - Q - P_u B_c R^{-1} B_c^T P_u\right) x. \tag{21}$$

If the following inequality holds for the considered ΔA:

$$P_u \Delta A + \Delta A^T P_u < P_u B_c R^{-1} B_c^T P_u + Q. \tag{22}$$

then x exponentially converges to zero.

Extensive simulation results considering parameter uncertainties will be included in Section 5.

4. High-order optimal disturbance observer-based control

This section presents the designing of the proposed high-order optimal observer for estimating aerodynamic torque as rapidly

changing disturbances. To estimate T_a, the speed dynamics equation in (6) is considered:

$$\dot{\omega} = \left(-\frac{B}{J}\omega - \frac{1}{J}T_e + \frac{1}{Jn_{gb}}T_a\right) \tag{23}$$

Assumption 3: A disturbance term, defined as, $d = \frac{1}{Jn_{gb}}T_a$ is assumed to be continuous and its r^{th} -order time-derivative is bounded, i.e., $|d^{(r)}| \leqslant \xi$, where $d^{(r)}$ is the r^{th}-order time derivative of the disturbance, and $\xi > 0$ represents an unknown number.

4.1. High-order optimal disturbance observer design

Combining (23) and *Assumption 2*, the following extended system can be achieved:

$$\begin{cases} \dot{\bar{x}} = \bar{A}\bar{x} + \bar{B}u + \bar{M}d^{(r)} \\ y = \bar{C}\bar{x} \end{cases} \tag{24}$$

where $\bar{x} = \begin{bmatrix} \omega & d & d^{(1)} & \cdots & d^{(r)} \end{bmatrix}^T, u = -\frac{1}{J}T_e,$

$$\bar{A}_{(r+1)\times(r+1)} = \begin{bmatrix} -\frac{B}{J} & 1 & 0 & \cdots & 0 \\ 0 & 0 & 1 & \cdots & 0 \\ \vdots & & & & \\ 0 & 0 & 0 & \cdots & 1 \\ 0 & 0 & 0 & \cdots & 0 \end{bmatrix}, \bar{B}_{(r+1)\times 1} = \begin{bmatrix} 1 \\ 0 \\ \vdots \\ 0 \end{bmatrix}, \tag{25}$$

$$\bar{C}_{1\times(r+1)} = [1 \quad 0 \quad \cdots \quad 0], \bar{M}_{(r+1)\times 1} = \begin{bmatrix} 0 \\ 0 \\ \vdots \\ 1 \end{bmatrix},$$

It is straightforwarded to see that for any positive integer value of r a pair $\left(\bar{A}, \bar{C}\right)$ is observable.

The proposed high-order optimal disturbance observer is designed as:

$$\frac{d\hat{\bar{x}}}{dt} = \bar{A}\hat{\bar{x}} + \bar{B}u + L_g\left(y - \bar{C}\hat{\bar{x}}\right) \tag{26}$$

where $L_g = P_0\bar{C}^T R_0^{-1}$ is the observer gain with P_0 as the solution of the ARE below:

$$\bar{A}P_0 + P_0\bar{A}^T - P_0\bar{C}^T R_0^{-1}\bar{C}P_0 + Q_0 = 0 \tag{27}$$

where $Q_0 \geqslant 0, R_0 > 0$ and both are symmetric matrices.

The error dynamics form of the proposed observer is obtained as:

$$\frac{d\tilde{\bar{x}}}{dt} = \left(\bar{A} - L_g\bar{C}\right)\tilde{\bar{x}} + \bar{M}d^{(r)} \tag{28}$$

where $\tilde{\bar{x}}$ is the estimation error, $\tilde{\bar{x}} = \bar{x} - \hat{\bar{x}}$.

Theorem 2. The proposed high-order optimal disturbance observer (HOODO) designed with (26)–(27) can guarantee a bounded estimation error.

Proof. Let us introduce a Lyapunov function as $V\left(\tilde{\bar{x}}\right) = \tilde{\bar{x}}^T G\tilde{\bar{x}}$, where $G = P_0^{-1}$. The first-order time-derivative of the candidate Lyapunov function written in terms of the observer's error dynamics (28) is determined by

$$\begin{aligned} &\dot{V} = \tfrac{d}{dt}\tilde{\bar{x}}^T G\tilde{\bar{x}} = 2\tilde{\bar{x}}^T\left(G\bar{A} - P_0C^T R^{-1}C\right)\tilde{\bar{x}} + 2\tilde{\bar{x}}^T G\bar{M}d^{(r)} = \\ &\tilde{\bar{x}}^T G\left(\bar{A}P_0 + P_0\bar{A}^T - 2P_0\bar{C}^T R^{-1}\bar{C}P_0\right) \times G\tilde{\bar{x}} + 2\tilde{\bar{x}}^T G\bar{M}d^{(r)} \leqslant \\ &-\tilde{\bar{x}}^T GQ_0G\tilde{\bar{x}} + 2\tilde{\bar{x}}^T G\bar{M}d^{(r)} \leqslant -\|\tilde{\bar{x}}\|\left(\lambda_{m1}\|\tilde{\bar{x}}\| - 2\|G\bar{M}\|\varepsilon\right) \end{aligned} \tag{29}$$

where λ_{m1} denote the smallest eigenvalue of GQ_0G. Therefore, an appropriate tuning of Q_0 and R_0 can provide a bounded norm of the estimator after sufficiently large duration of time, i. e.

$$\|\tilde{\bar{x}}\| \leqslant \lambda_1 \tag{30}$$

where $\lambda_1 = 2\|H\bar{M}\|\varepsilon/\lambda_{m1}$.

We note that the estimation performance of the observer depends on the value of λ_1. Its value can be selected by changing Q_0 and R_0. Hence, by referring to [47], the observer can guarantee definitive boundedness and uniform stability of a small ball with the center at $\tilde{\bar{x}} = 0$.

Remark 1: In a previous work [48], a high-order observer (HOO) was presented to estimate the high-order disturbance with the assumption that $d^{(r)} = 0$. This somehow solves the conventional assumption associated with conventional DO that $d^{(1)} = \dot{d} = 0$; however, does not reflect a broad range of time-varying disturbance, such as that in aforementioned *Assumption 1*. For example, when the disturbance includes a fast-varying sinusoidal signal, the assumption in HOO is not applicable.

Remark 2: The gains in HOO is designed based on a loose guideline, in which the observer gains are selected such that the characteristic equation meets the Hurwitz criterion. That means as long as the gains are positive, it is satisfied. This does not help the designer to select appropriate gains for their applications other than trial-and-error. On the other hand, the proposed HOODO is designed based on the optimal control framework, has a systematic way of selecting the weighting matrices, i.e., selecting the gains of the observer via an straight-forward and implementable rule.

4.2. High-order optimal disturbance observer-based tracking control

With $\hat{d} = \frac{1}{Jn_{gb}}\hat{T}_a$ estimated by using the HOODO and the system as in (11); via (1), (3), (5) and (10), the estimation of the generator's reference speed is calculated as

$$\hat{\omega}_{ref} = n_{gb}\sqrt{\frac{\hat{T}_a}{k_{opt}}} \tag{31}$$

where $k_{opt} = \frac{1}{2}\rho\pi R^5\frac{C_{pmax}}{\lambda_{opt}^3}$. Based on estimated aerodynamic torque $\hat{T}_a$, the compensating terms as well as reference speed tracking error are derived as

$$\begin{aligned} &\tilde{\hat{\omega}} = \omega - \hat{\omega}_{ref}; \tilde{\hat{T}}_e = T_e - \hat{T}_{e_{ref}}; \\ &\hat{T}_{e,ref} = \tfrac{1}{n_{gb}}\hat{T}_a - B\hat{\omega}_{ref} - J\dot{\hat{\omega}}_{ref} \\ &\hat{u}_{qc} = \tfrac{R_s}{K}\hat{T}_{e,ref} + \tfrac{L_s}{K}\dot{\hat{T}}_{e,ref} + \psi_m P\hat{\omega}_{ref} + PL_s\omega i_d \end{aligned} \tag{32}$$

Control law (15) now becomes

$$u = \hat{u}_c + K_u\hat{x} \tag{33}$$

where $\hat{x} = \begin{bmatrix} \tilde{\hat{\omega}} & \tilde{\hat{T}}_e & \tilde{i}_d \end{bmatrix}^T, \hat{u}_c = \begin{bmatrix} \hat{u}_{qc} & u_{dc} \end{bmatrix}^T$.

Then, from (31)–(33), the following equations are achieved,

$$\begin{aligned} \hat{x} &= x + Fx_e \\ \hat{u}_c &= u_c + Hx_e \end{aligned} \tag{34}$$

where

$$x_e = [e \quad \dot{e}]^T, e = T_a - \hat{T}_a, F = \begin{bmatrix} n_1 & n_2 & 0 \\ 0 & 0 & 0 \end{bmatrix}^T, H = \begin{bmatrix} n_3 & n_4 \\ 0 & 0 \end{bmatrix}.$$

$$n_1 = \frac{n_{gb}}{\sqrt{k_{opt}}\left(\sqrt{T_a} + \sqrt{T_a}\right)}, \qquad n_2 = \frac{1}{n_{gb}} - Bn_1 - Jg, \qquad \text{with}$$

$$g = \frac{n_{gb}}{2\sqrt{k_{opt}T_a\hat{T}_a}}\left(\sqrt{T_a} - \frac{\hat{T}_a}{T_a + T_a}\right),$$

$$n_3 = -\frac{R_s n_2}{K} + \frac{LB}{K}\dot{g} - \psi_m P n_1,\ n_4 = -\frac{L_s}{K}\left(\frac{1}{n_{gb}} - Jg\right).$$

4.3. Closed-loop stability analsysis

Let us rewrite (33) based on (34) as

$$u = u_c + K_u x + E x_e \tag{35}$$

where $E = K_u F + H$.

On the other hand, we have

$$x_e = U\tilde{\bar{x}} \tag{36}$$

where $U_{2\times(r+1)} = \begin{bmatrix} 0 & 1 & 0\cdots & 0 \\ 0 & 0 & 1\cdots & 0 \end{bmatrix}$.

Theorem 3. A state vector x and its estimation error $\tilde{\bar{x}}$ are ultimately bounded around the origin.

Proof. Let us take a Lyapunov function of the form:

$$V\left(x, \tilde{\bar{x}}\right) = x^T P_u x + \gamma \tilde{\bar{x}}^T G \tilde{\bar{x}} \tag{37}$$

where $\gamma > 0$.

The time-derivative of the Lyapunov function is

$$\begin{aligned} &\dot{V}(x, x_e) = 2x_T P_u (Ax + B_c u - B_c u_c) + 2\gamma \tilde{\bar{x}}^T G\left(\bar{A} - L_g \bar{C}\right)\tilde{\bar{x}} = \\ &2x_T P_u \left(Ax - B_c K_u x + B_c E U \tilde{\bar{x}}\right) + 2\gamma \tilde{\bar{x}}^T G\left(\bar{A} - L_g \bar{C}\right)\tilde{\bar{x}} + 2\gamma \tilde{\bar{x}}^T G \overline{M d^{(r)}} \leqslant \\ &-x^T Q x + 2x^T P_u B_c E U \tilde{\bar{x}} - \gamma \tilde{\bar{x}}^T G Q_0 G \tilde{\bar{x}} + 2\gamma \tilde{\bar{x}}^T G \bar{M} \varepsilon \end{aligned} \tag{38}$$

We further denote $x_a = \begin{bmatrix} x & \tilde{\bar{x}} \end{bmatrix}^T$, so

$$x = T_1 x_a, \tilde{\bar{x}} = T_2 x_a \tag{39}$$

where $T_1 = \begin{bmatrix} I_3 & 0_{3\times(r+1)} \end{bmatrix}, T_2 = \begin{bmatrix} 0_{(r+1)\times 3} & I_{(r+1)} \end{bmatrix}$.

Then,

$$\begin{aligned} &-x^T Q x + 2x_T P_u B_c E U \tilde{\bar{x}} - \gamma \tilde{\bar{x}}^T G Q_0 G \tilde{\bar{x}} + 2\gamma \tilde{\bar{x}}^T G \bar{M} \varepsilon = \\ &-x_a^T T_1^T Q T_1 x_a + 2x_a^T T_1^T P_u B_c E U T_2 X_a - \gamma x_a^T T_2^T G Q_0 G T_2 x_a + 2\gamma x_a^T T_2^T G \bar{M} \varepsilon \leqslant \\ &-\lambda_{m2} \|x_a\|^2 + 2\gamma \|T_1^T P_u B_c E U T_2\| \cdot \|x_a\|^2 + 2\gamma \varepsilon \|T_2^T G \bar{M}\| \|x_a\| = \\ &-\|x_a\| \left[\left(\lambda_{m2} - 2\gamma \|T_1^T P_u B_c E U T_2\| \right) \|x_a\| - 2\gamma \varepsilon \|T_2^T G \bar{M}\| \right] \end{aligned} \tag{40}$$

where λ_{m2} denote the smallest eigenvalue of $\left(T_1^T Q T_1 + \gamma T_2^T G Q_0 G T_2\right)$. From (40), it is seen that we can always obtain γ to assure that

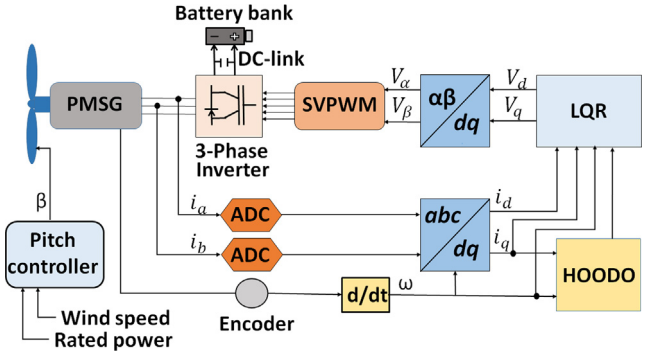

Fig. 2. General control scheme of the PMSG-based WECS with the proposed HOODO-based LQR.

Table 1
Parameters of the WECS [49].

Symbol	Quantity	Value	[Unit]
P_{rated}	Rated power	5	kW
R_s	Resistance of a stator	0.3676	Ω
L_s	Inductance of a stator	3.55	mH
ψ_m	Magnet flux linkage	0.2867	$V \cdot s/rad$
J	Mechanical inertia	7.856	$kg \cdot m^2$
P	Pole pairs	14	–
B	Viscous friction coefficient	0.002	$kg \cdot m^2/s$
R	Rotor radius	1.84	m
ρ	Air density	1.25	kg/m^3
n_{gb}	Gear box ratio	1	–

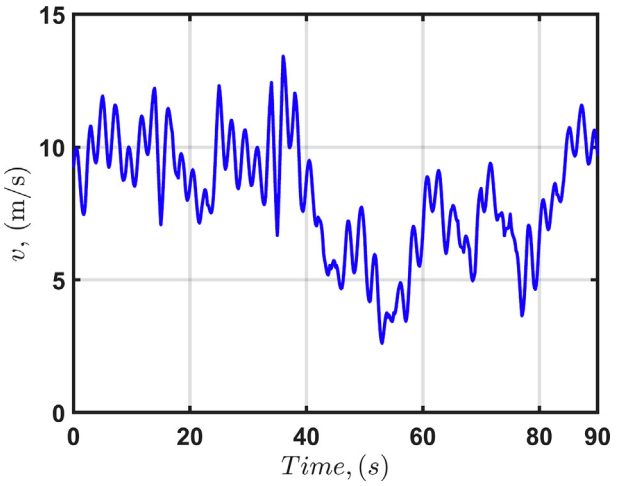

Fig. 3. Wind profile used in the study.

Table 2
Parameters of controllers and observers.

	Parameters
LQR	$Q = diag(1e5, 1, 1), R = diag(1, 1)$
HOODO, $r = 1$	$Q = 5e2 \times diag(1e1, 1), R = 1$
HOODO, $r = 2$	$Q = 5e2 \times diag(1e1, 1e2, 1), R = 1$
HOODO, $r = 3$	$Q = 5e2 \times diag(1e1, 1e2, 1e2, 1), R = 1$
HOODO, $r = 4$	$Q = 5e2 \times diag(1e1, 1e2, 1e2, 1e2, 1), R = 1$
HOO, $r = 1$	$L_0 = 1e2, L_1 = 1e3$
HOO, $r = 2$	$L_0 = 1e2, L_1 = 1e3, L_2 = 3e4$
HOO, $r = 3$	$L_0 = 1e2, L_1 = 1e3, L_2 = 3e4, L_3 = 1e1$
HOO, $r = 4$	$L_0 = 1e2, L_1 = 1e3, L_2 = 3e4, L_3 = 1e1, L_4 = 1e1$

Table 3
Tracking error of the reference speed.

		Scenario 1	Scenario 2	Scenario 3	Scenario 4
$\Delta R_s, \%$		0	+20	+40	+40
$\Delta L_s, \%$		0	−1	−15	−15
$\Delta\psi_m, \%$		0	0	0	−2
$\tilde{\omega}_{LQR+HOO}, rad/s$	$r = 1$	19.0570	18.8910	23.6818	22.6737
	$r = 2$	2.6650	2.6022	3.6882	3.5078
	$r = 3$	2.6650	2.6022	3.6883	3.5085
	$r = 4$	2.6650	2.6022	3.6883	3.5085
$\tilde{\omega}_{LQR+HOODO}, rad/s$	$r = 1$	9.1160	9.0555	11.7513	11.2662
	$r = 2$	0.4724	0.4726	0.4715	0.4717
	$r = 3$	0.4822	0.4823	0.4813	0.4815
	$r = 4$	0.4713	0.4714	0.4703	0.4706

$\left(\lambda_{m2} - 2\gamma\|T_1^T P_u B_c E U T_2\|\right) > 0$. So, after sufficiently long time with appropriately selected Q_0, R_0, Q, and R, $\|x_a\|$ is bounded as

$$\|x_a\| \leqslant \lambda_2 \tag{41}$$

where $\lambda_2 = 2\gamma\varepsilon\|T_2^T G\overline{M}\|/\left(\lambda_{m2} - 2\gamma\|T_1^T P_u B_c E U T_2\|\right)$. Hence, the state vector x and its estimation error $\tilde{x}$ are bounded, and by appropriate tuning of the weighting matrices of both controller and observer, it is possible to lower that bound. Finally, the stability of closed-loop composite control based on the HOODO is proven in the sense of [47].

5. Simulation results

The control scheme of the PMSG-based WECS is shown in Fig. 2. The diagram includes a PMSG, a three-phase inverter, a DC-link with battery bank. The control system requires an encoder and two current sensors. The signals of current is fed to analog-to-digital (ADC) block. There are also Clark and Park blocks required for the frame transformations. The control system includes the proposed HOODO and LQR. The output of controller is then sent to a block for frame transformation and then to the space vector pulse-width modulation (SVPWM) to generate high-frequency switching commands for the three phase inverter. A pitch controller is designed to prevent the WECS system from damage when the wind speed is above the rated value.

The WECS parameters are shown in Table 1. On the other hand, a profile of the time-varying wind speed, with an average speed equals to 8.43 m/s, is depicted in Fig. 3. The profile has been generated by adding four periodic signals with various amplitudes and frequencies and a Gaussian noise. The generated wind profile signal varies rapidly from a minimum equal to 2.6 m/s to a maximum equal to 14.4 m/s. The maximum power factor $C_{p_{max}} = 0.4412$ was calculated using $\lambda_{opt} = 8.09$.

Table 2 shows the selected weighting matrices of the LQR, proposed HOODO, and HOO [50].

5.1. Discussion of results

Two control schemes are tested under four different scenarios, where performances of the HOO and HOODO are compared for variations in L_s, R_s, and ψ. In Scenario 1, we studied performance of each control scheme applied for the WECS with nominal values of each parameter (L_s, R_s, ψ). In Scenario 2, we applied the HOO and HOODO for the WECS where the stator inductance L_s decreased by -1 % and the stator resistance R_s increased by 20 %, whereas the magnetic flux linkage ψ remained to be constant. Scenario 3 considers parameter variations similar to [50], where the stator inductance decreased by 15 % and resistance increased by 40 %, while the magnetic flux linkage did not change. In Scenario 4, the variations in the stator resistance and inductance are taken similar to the amount of variations in Scenario 3, and the magnetic flux linkage is decreased by -2 % with assumption that the motor operates under high temperature for a long time [51,52]. The results of each scenario are summarized in Table 3 and Table 4. Here, the HOO [50] is implemented with the same controller and the same scenarios for the purpose of comparison.

Figs. 4–15 present the simulation results of the proposed HOODO-based LQR method under Scenario 2. Figs. 6, 7 illustrate

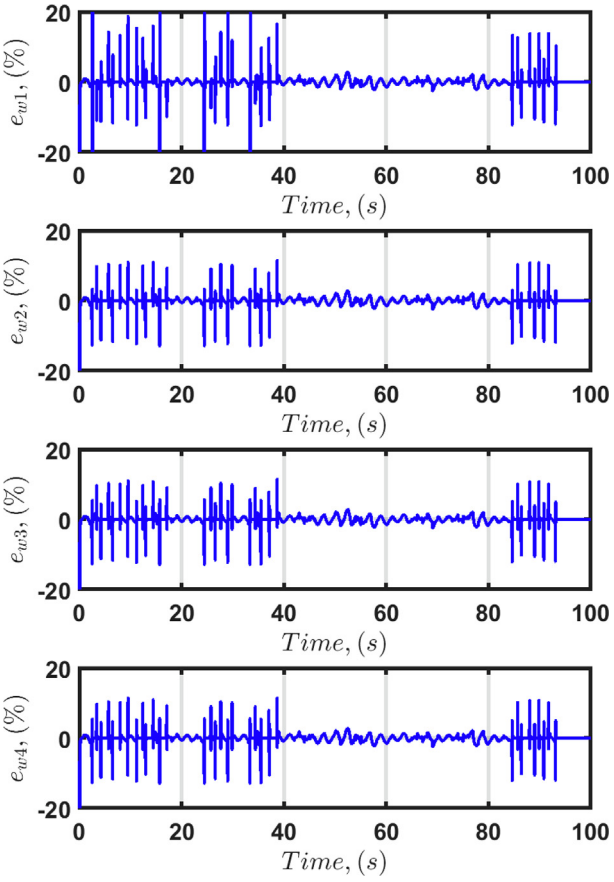

Fig. 4. Scenario 2. Errors of speed estimation with the HOODO-based LQR for $r = 1, 2, 3, 4$.

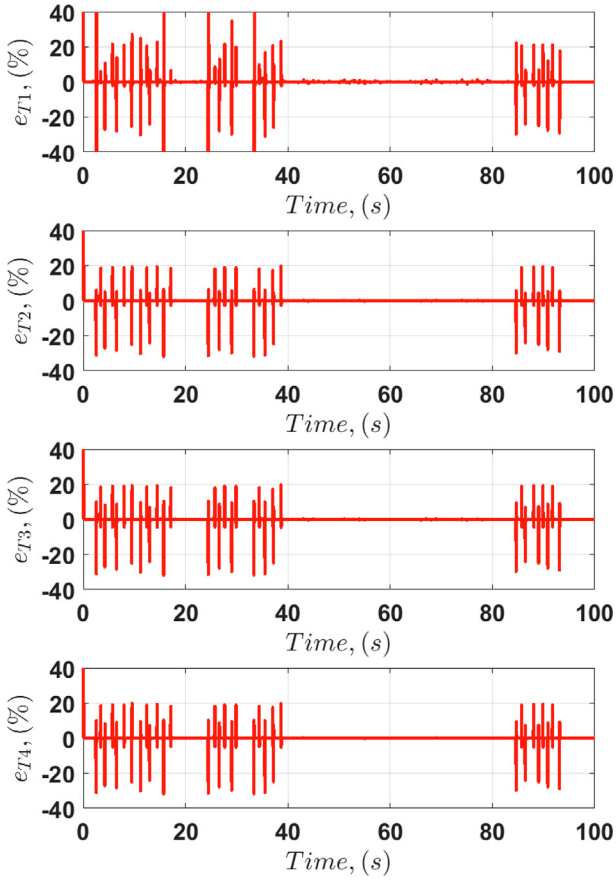

Fig. 5. Scenario 2. Errors of aerodynamic torque estimation with the HOODO-based LQR for $r = 1, 2, 3, 4$.

Table 4
Tracking error of T_a.

		Scenario 1	Scenario 2	Scenario 3	Scenario 4
$\Delta R_s, \%$		0	+20	+40	+40
$\Delta L_s, \%$		0	−1	−15	−15
$\Delta\psi_m, \%$		0	0	0	−2
$\tilde{T}_{a_{LQR+HOO}}, N \cdot m$	$r=1$	1.5688	1.5666	1.6366	1.6329
	$r=2$	1.3932	1.3916	1.4284	1.4181
	$r=3$	1.3932	1.3916	1.4284	1.4181
	$r=4$	1.3932	1.3916	1.4284	1.4181
$\tilde{T}_{a_{LQR+HOODO}}, N \cdot m$	$r=1$	1.5149	1.5136	1.5908	1.5872
	$r=2$	0.6273	0.6273	0.6276	0.6276
	$r=3$	0.6896	0.6896	0.6900	0.6899
	$r=4$	0.6251	0.6251	0.6253	0.6253

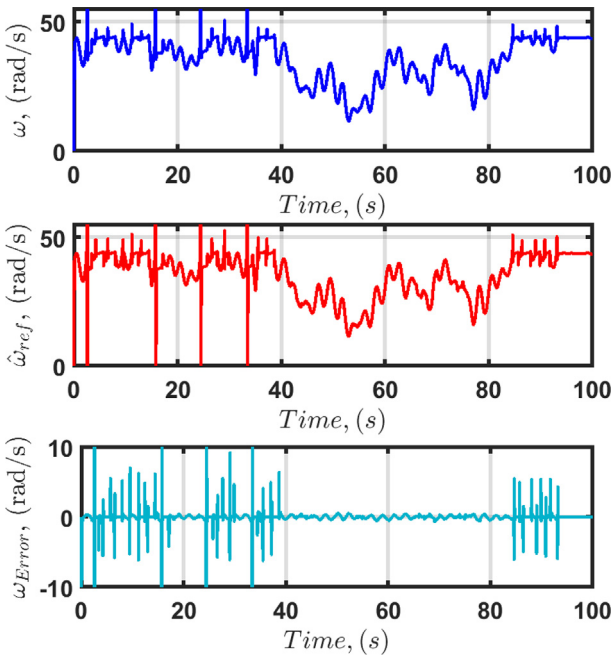

Fig. 6. Scenario 2. Speed tracking performance with the proposed HOODO-based LQR for $r = 1$.

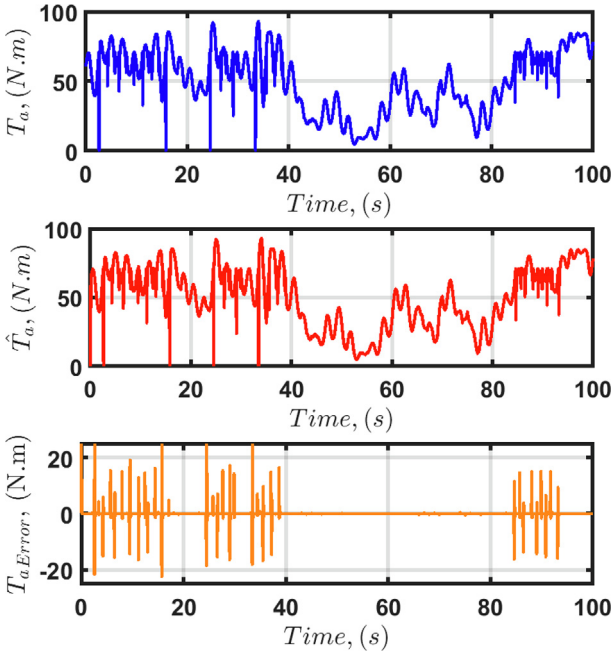

Fig. 7. Scenario 2. Estimation of T_a with the HOODO-based LQR for $r = 1$.

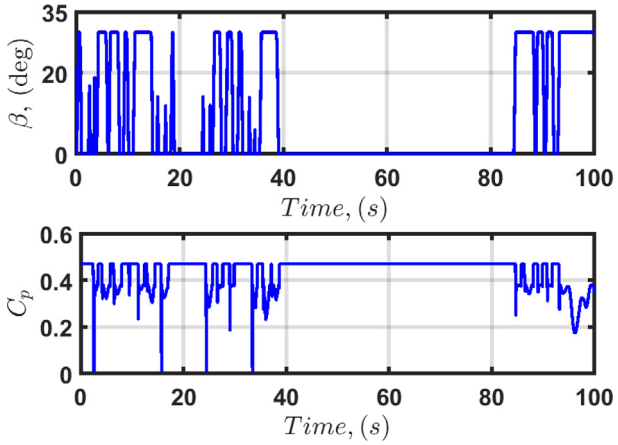

Fig. 8. Scenario 2. Pitch-angle and power coefficient with the proposed HOODO-based LQR for $r = 1$.

the controller and observer performance with the proposed HOODO-based LQR with $r = 1$. It is seen from these figures that the estimated T_a and tracking error are sufficiently accurate for the proposed LQR with HOODO observers. Fig. 8 presents the pitch angle control performance for $r = 1$. Figs. 9–17 show the estimation and control performances with $r = 2, r = 3$, and $r = 4$, respectively. Despite of the rapid change of the wind speed and pitch angle in this gust wind, the HOODO-based LQR is able to show its good performance in all cases. Figs. 18–21 illustrate the performance of the HOO for comparison. For the convenience of the reader to track the difference of these methods, Tables 3 and 4 summarize the results for each case. It can be seen that, as the order increase higher than two, the performance is slightly improved for both HOO and the proposed HOODO. Also, it is clear from the table that, with HOODO, both the wind speed tracking and disturbance estimation performances are better compared to those of the HOO. For example, with $r = 2$ in Scenario 1, the root

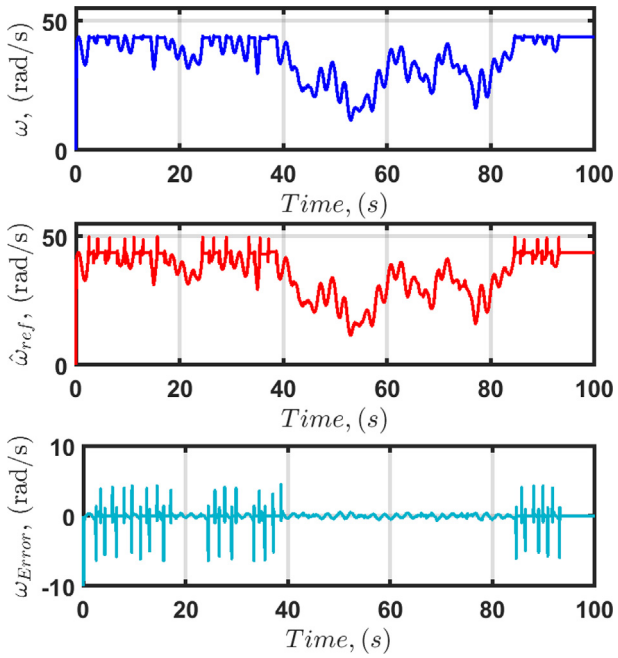

Fig. 9. Scenario 2. Speed tracking performance with the proposed HOODO-based LQR for $r = 2$.

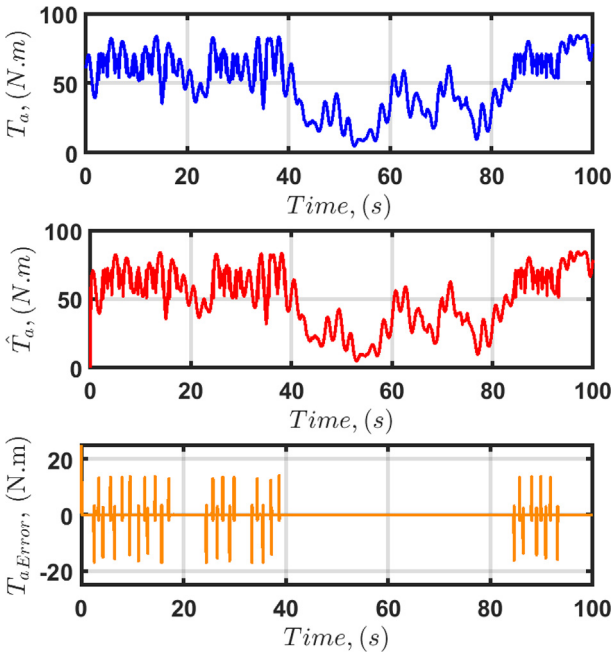

Fig. 10. Scenario 2. Estimation of T_a with the HOODO-based LQR for $r = 2$.

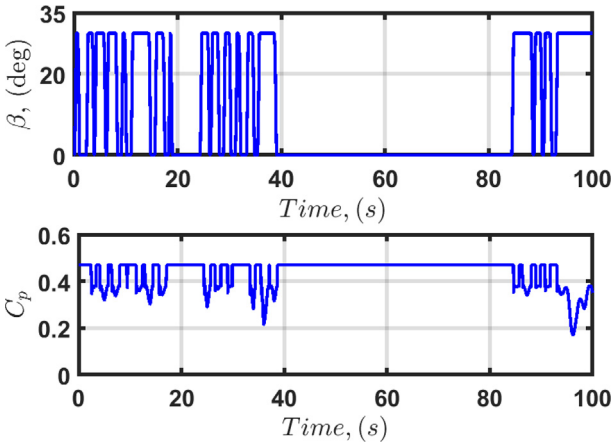

Fig. 11. Scenario 2. Pitch-angle and power coefficient with the proposed HOODO-based LQR for $r = 2$.

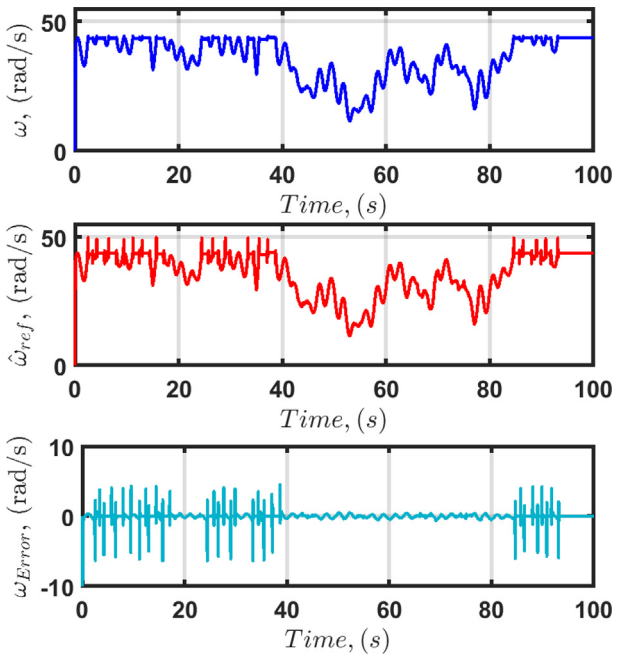

Fig. 12. Scenario 2. Speed tracking performance with the proposed HOODO-based LQR for $r = 3$.

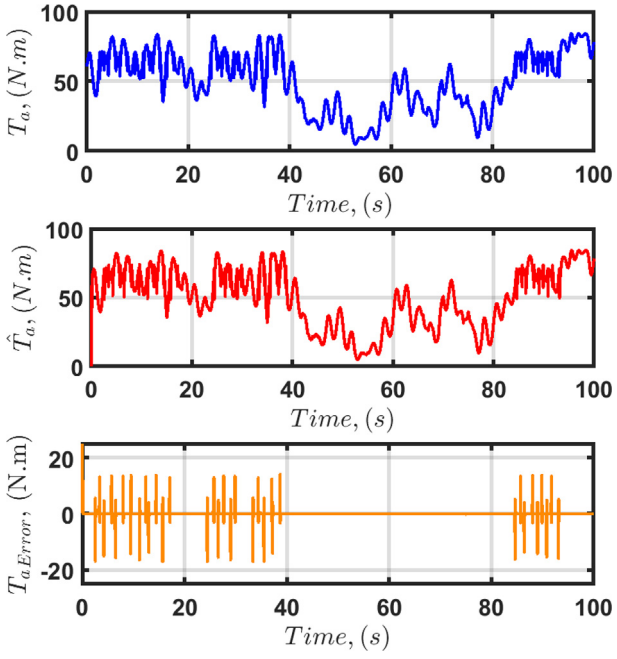

Fig. 13. Scenario 2. Estimation of T_a with the HOODO-based LQR for $r = 3$.

mean of squared error (RMSE) of the wind speed tracking and aerodynamic torque estimation with the proposed HOODO is 0.4724% and 0.6273%, respectively; whereas those with HOO are larger, 2.6650% of the wind speed tracking and 1.3932% of aerodynamic torque estimation. In Scenario 2, LQR with HOO shows the RMSE value of 2.6022% for the wind speed tracking and 1.3916% for aerodynamic torque estimation, whereas the RMSE values for the torque estimation and wind speed tracking for the proposed HOODO control scheme did not change from Scenario 1 to Scenario 2. In scenarios 3 and 4, we consider more severe condition by considering larger parameter variations. In both scenarious, the first order HOO and HOODO degrade in performance of speed estimation, and show more stable results starting from the order two. Nevertheless, starting from the second order, the HOODO gives much less estimation error comparing to the HOO, which means that the HOODO is more accurate than the HOO under the severe parameter variations.

Further comparison of the proposed HOODO with the HOO observer from the simulation results shows that for the HOO, the error in estimating the aerodynamic torque of four values of r for the HOO-based LQR control scheme are $(e_T)_{max} = 1.5688\%$, 1.3932% and $1.3932\%, 1.3932\%$ for $r = 1, 2, 3$ and 4, respectively. For the wind speed estimation error $(\tilde{\omega})_{max} = 19.0570\%, 2.6650\%$ and $2.6650\%, 2.6650\%$ for $r = 1, 2, 3$ and 4, respectively. While the HOODO-based LQR control results show that the aerodynamic torque estimation error and angular speed estimation error are

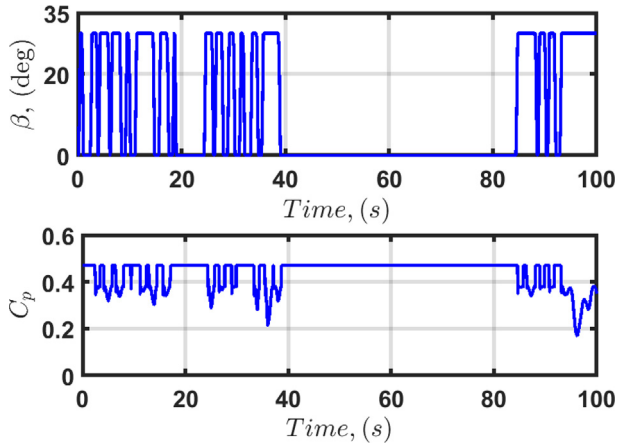

Fig. 14. Scenario 2. Pitch-angle and power coefficient with the proposed HOODO-based LQR for $r = 3$.

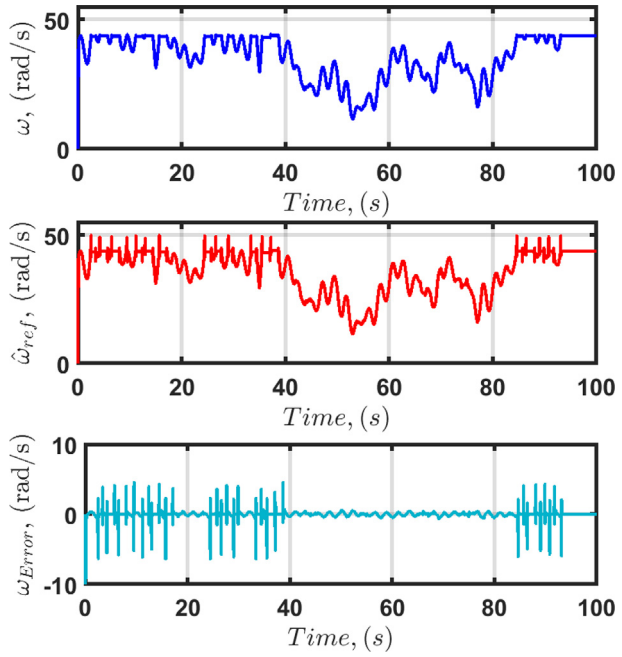

Fig. 15. Scenario 2. Speed tracking performance with the proposed HOODO-based LQR for $r = 4$.

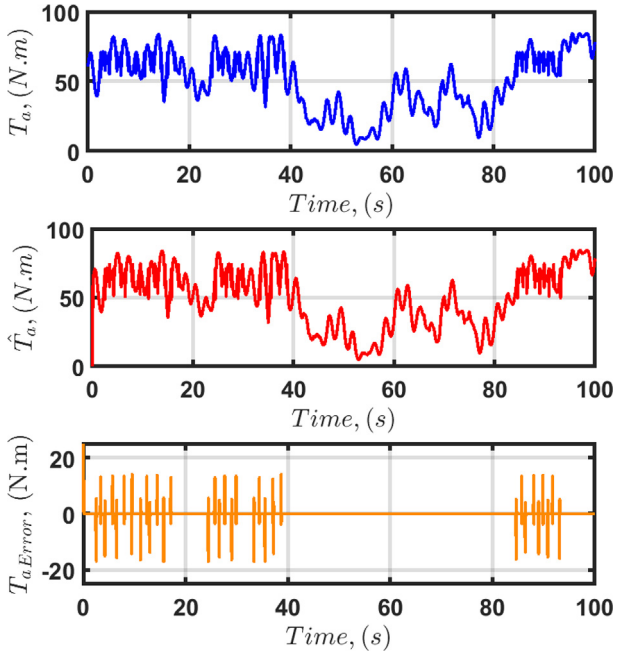

Fig. 16. Scenario 2. Estimation of T_a with the HOODO-based LQR for $r = 4$.

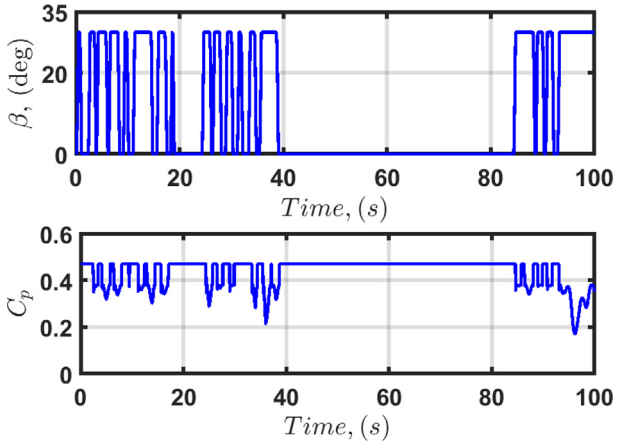

Fig. 17. Scenario 2. Pitch-angle and power coefficient with the proposed HOODO-based LQR for $r = 4$.

unchanged for all $r = 1, 2, 3$ and $4 : (e_T)_{max} = 9.1160\%, 0.4724\%, 0.4822\%, 0.4713\%$ and $(\tilde{\omega})_{max} = 1.5149\%, 0.6273\%, 0.6896\%, 0.6251\%$, respectively, and are illustrated in Fig. 4. The aerodynamic torque estimation errors for each r are plotted in Fig. 5. By looking at the aerodynamic torque estimation performance in Table 4, one can conclude that the proposed HOODO scheme can be used to achieve much less estimation error than the HOO. Further, to validate robustness of the HOODO performance to different parameter variations, we run 10 random simulations with the same wind profile for all cases, where R_s is randomly increases in the range $[1\%, 40\%]$, L_s, and ψ_m randomly decrease in the range $[-15\%, 0\%]$ and $[-2\%, 0\%]$, respectively. The amount of variations for each parameter were determined using a uniform probability distribution within the given ranges. The simulation results of speed estimation error and aerodynamic torque estimation error are respectively shown in Tables 5 and 6. The estimation performance for both speed and aerodynamic shows that the HOODO can guarantee a stable estimation error with amplitude less than 0.5 *rad/s* and 0.7 *rad/s* for the speed and aerodynamic estimation error, respectively.

It can be revealed from the results that the use of HOODO-based LQR can significantly improve a system performance by reducing the tracking error comparing to the HOO-based LQR in both cases. It means the designed HOODO-based LQR method is more robust to changes in the system and parameters uncertainties. Moreover, by using of the designed HOODO-based control scheme, the estimation of ω and T_a in the PMSG-based WECS shows better results even in the cases of changing some parameters than the results reported in [35,36,40].

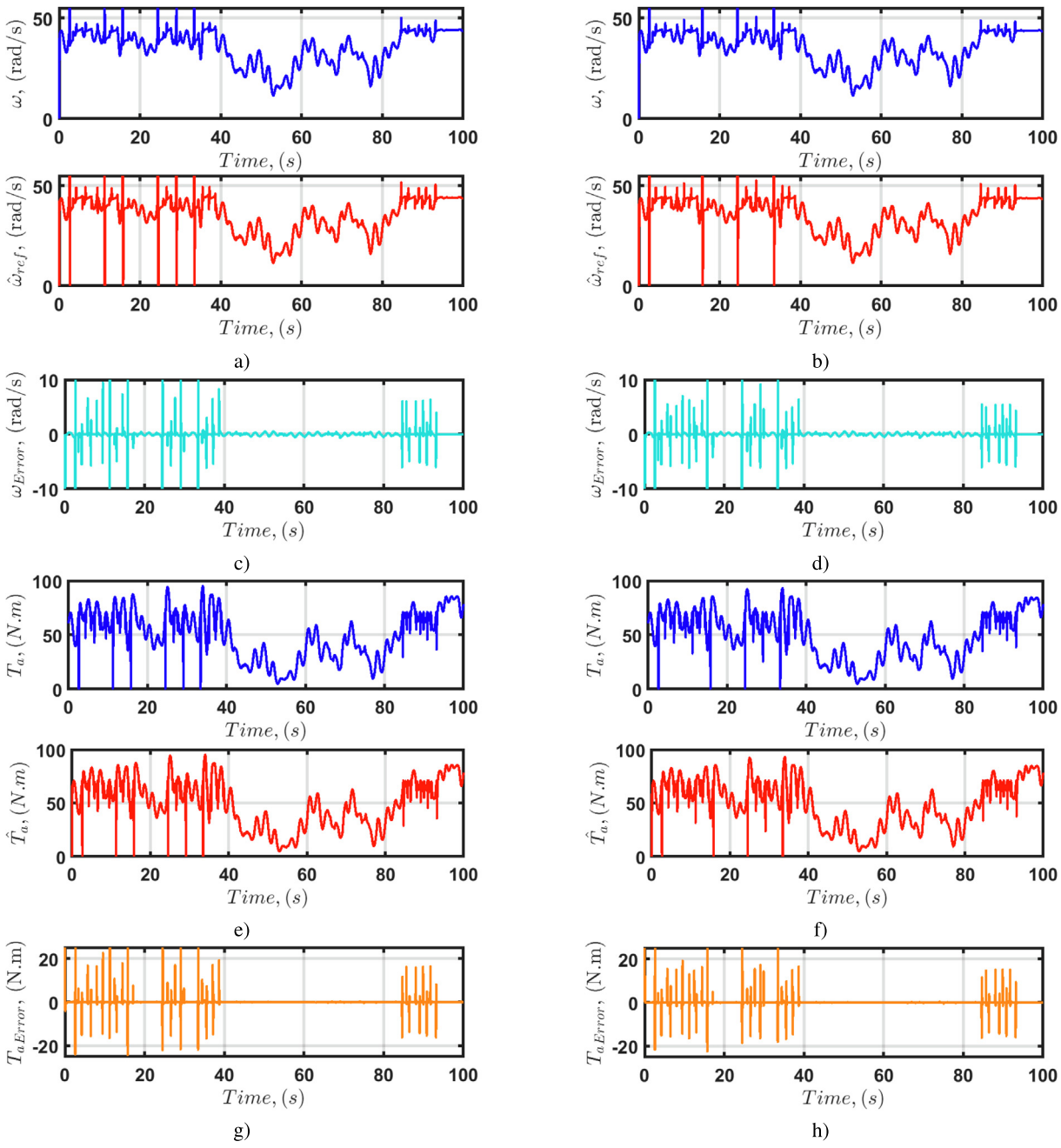

Fig. 18. Scenario 2. Tracking of reference wind speed and aerodynamic torque estimation performance for $r = 1$: a) Speed estimation with HOO; b) Speed estimation with HOODO; c) Speed estimation error with HOO; d) Error of the speed estimation with HOODO; e) Estimation of T_a with HOO; f) Estimation of T_a with HOODO; g) Estimation error of T_a with HOO; h) Estimation error of T_a with HOODO.

6. Conclusions

This work introduced the high-order optimal disturbance observer (HOODO)-based LQR for PMSG-based WECSs. The presented HOODO is able to estimate an aerodynamic torque considered as a disturbance and, hence, a speed of the wind with fast varying dynamics. Detailed analysis on the stability of the HOODO-based composite controller is carried out via the Lyapunov approach. The simulations show that the HOODO-based LQR has better accuracy than HOO-based LQR method. The presented controller with HOODO can guarantee smaller error and faster response time than previous observer-based control schemes reported so far. In addition, its parameter insensitivity property is significantly better than that of the HOO-based LQR. The work performed confirms the effectiveness of the proposed HOODO and its superiority compared to other types of high-order observers. Future work might focus on: 1) building an experimental setup and verify the performance of the proposed methods exper-

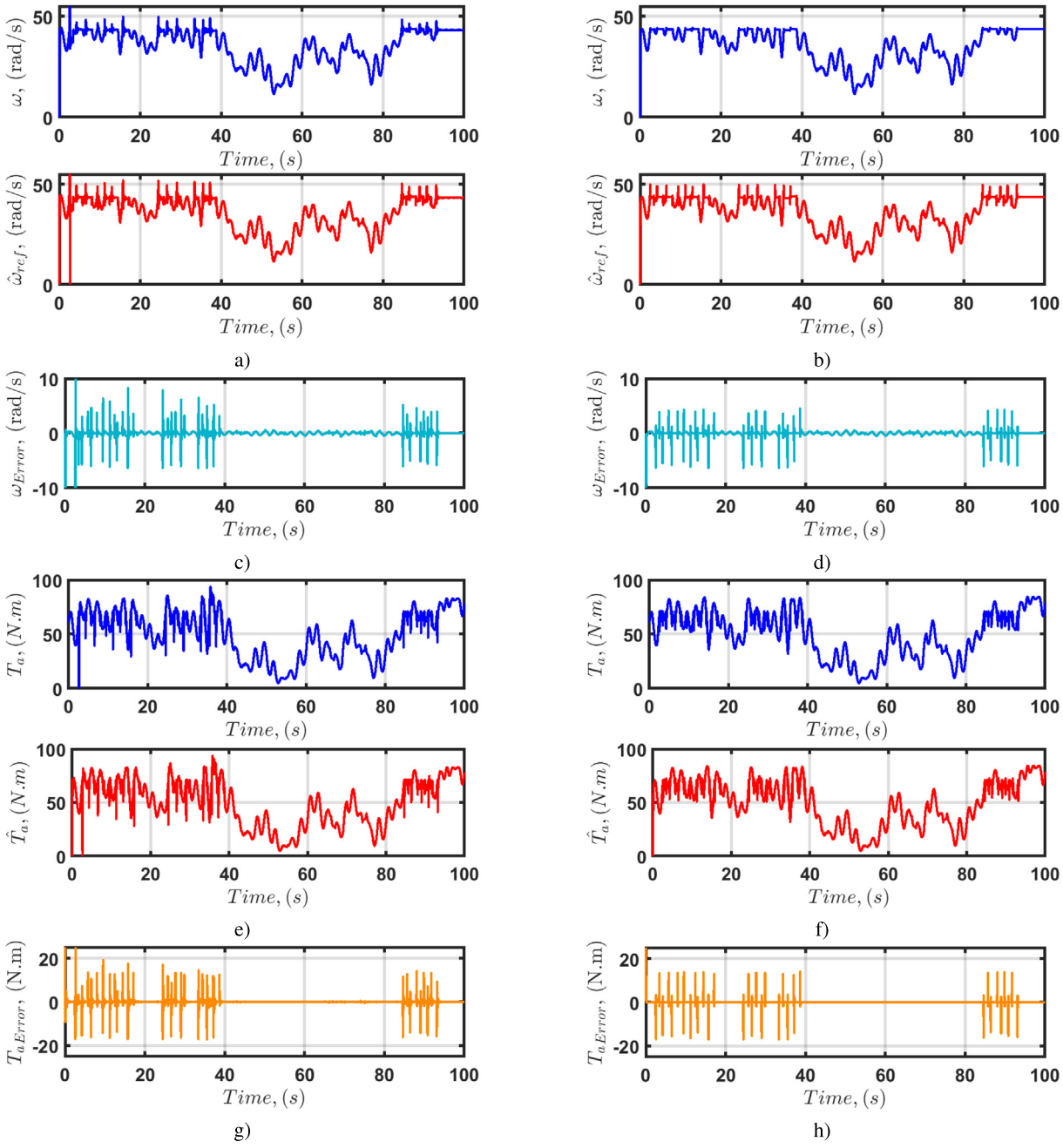

Fig. 19. Scenario 2. Tracking of reference wind speed and aerodynamic torque estimation performance for $r = 2$: a) Speed estimation with HOO; b) Speed estimation with HOODO; c) Speed estimation error with HOO; d) Error of the speed estimation with HOODO; e) Estimation of T_a with HOO; f) Estimation of T_a with HOODO; g) Estimation error of T_a with HOO; h) Estimation error of T_a with HOODO.

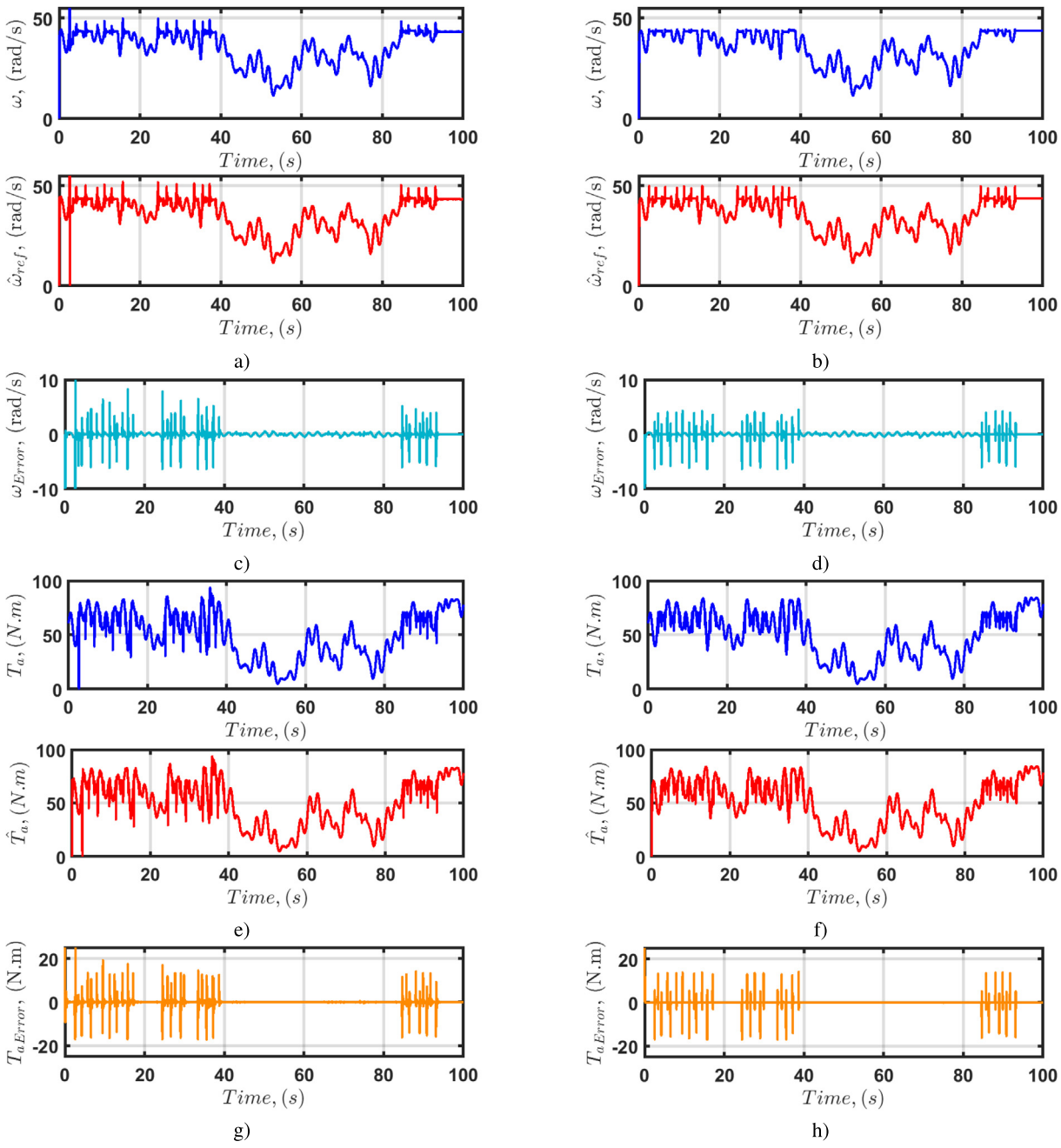

Fig. 20. Scenario 2. Tracking of reference wind speed and aerodynamic torque estimation performance for $r = 3$: a) Speed estimation with HOO; b) Speed estimation with HOODO; c) Speed estimation error with HOO; d) Error of the speed estimation with HOODO; e) Estimation of T_a with HOO; f) Estimation of T_a with HOODO; g) Estimation error of T_a with HOO; h) Estimation error of T_a with HOODO.

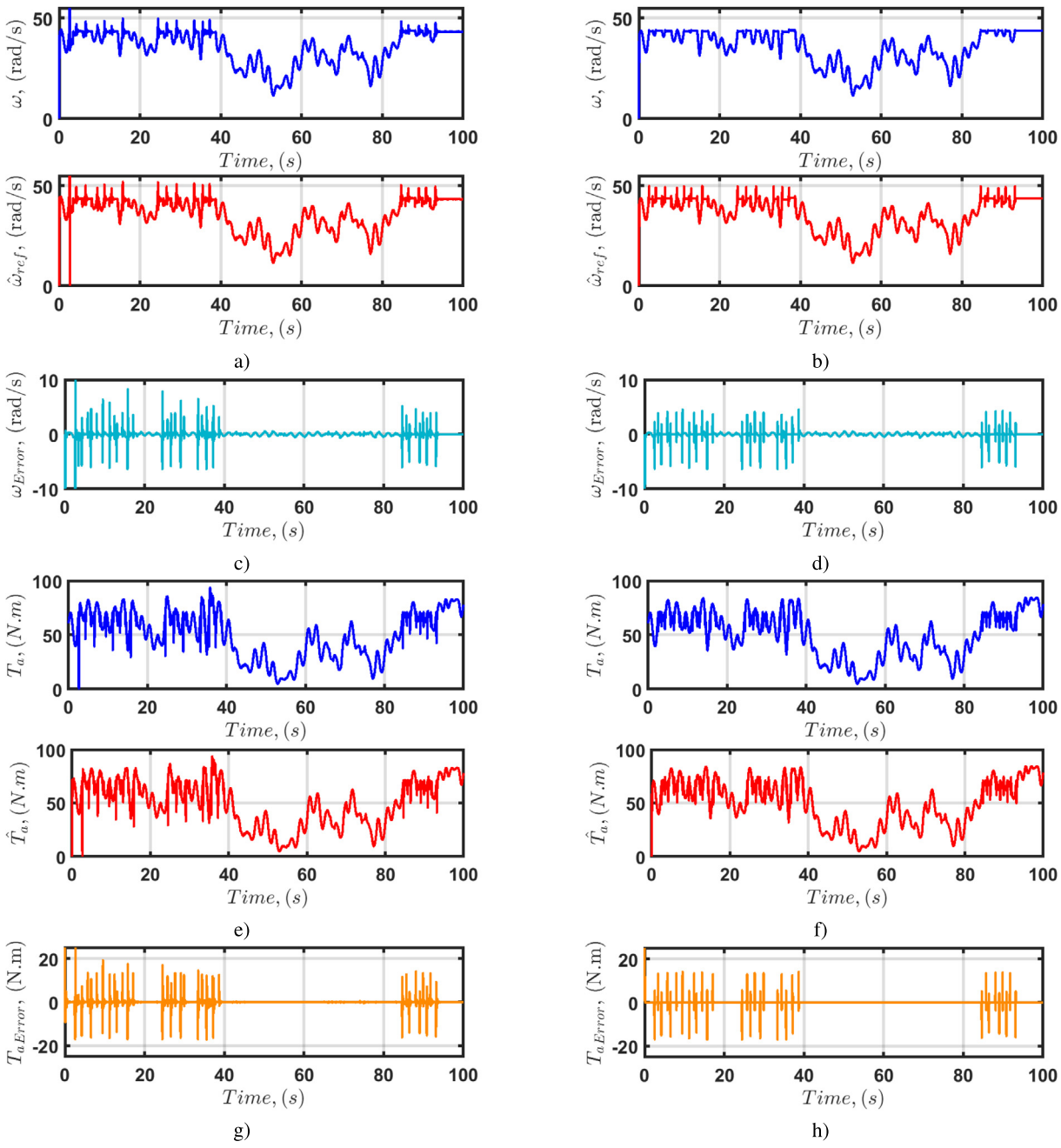

Fig. 21. Scenario 2. Tracking of reference wind speed and aerodynamic torque estimation performance for $r = 4$: a) Speed estimation with HOO; b) Speed estimation with HOODO; c) Speed estimation error with HOO; d) Error of the speed estimation with HOODO; e) Estimation of T_a with HOO; f) Estimation of T_a with HOODO; g) Estimation error of T_a with HOO; h) Estimation error of T_a with HOODO.

Table 5
Tracking error of the reference speed for 10 simulations with random parameter variations in the defined ranges.

Parameters		Simulations									
		1	2	3	4	5	6	7	8	9	10
$\Delta R_s, \%$		+22	+7	+25	+11	+27	+30	+19	+35	+17	+33
$\Delta L_s, \%$		−12	−15	−2	−9	−8	−6	−3	−14	−4	−10
$\Delta\psi_m, \%$		−1.9	−0.3	−1.7	−1.1	−2	−0.9	−0.2	−0.5	−1.5	−1.3
$\bar{\omega}_{LQR+HOODO}, rad/s$	$r=1$	11.1011	12.1692	8.7026	10.8419	9.6300	9.7866	9.5824	11.1827	9.3662	10.4607
	$r=2$	0.4717	0.4711	0.4728	0.4717	0.4723	0.4722	0.4723	0.4717	0.4724	0.4720
	$r=3$	0.4815	0.4809	0.4825	0.4815	0.4821	0.4820	0.4820	0.4815	0.4821	0.4818
	$r=4$	0.4705	0.4699	0.4717	0.4706	0.4712	0.4711	0.4712	0.4706	0.4713	0.4709

Table 6
Tracking error of T_a for 10 simulations with random parameter variations in the defined ranges.

Parameters		Simulations									
	1	2	3	4	5	6	7	8	9	10	
$\Delta R_s, \%$		+22	n+7	+25	+11	+27	+30	+19	+35	+17	+33
$\Delta L_s, \%$		−12	−15	−2	−9	−8	−6	−3	−14	−4	−10
$\Delta\psi_m, \%$		−1.9	−0.3	−1.7	−1.1	−2	−0.9	−0.2	−0.5	−1.5	−1.3
$\widetilde{T}_{a_{LQR+HOODO}}, N \cdot m$	$r=1$	1.5862	1.5946	1.5090	1.5843	1.5221	1.5259	1.5216	1.5866	1.5179	1.5803
	$r=2$	0.6275	0.6276	0.6273	0.6275	0.6274	0.6274	0.6274	0.6275	0.6274	0.6275
	$r=3$	0.6899	0.6901	0.6895	0.6899	0.6897	0.6897	0.6897	0.6899	0.6897	0.6898
	$r=4$	0.6253	0.6253	0.6251	0.6252	0.6252	0.6252	0.6252	0.6253	0.6251	0.6252

imentally. 2) Developing a finite time stability theory for closed-loop observer-based control for WECSs.

References

[1] Liao M, Dong L, Jin L, Wang S. Study on Rotational Speed Feedback Torque Control for Wind Turbine Generator System. 2009 International Conference on Energy and Environment Technology 2009; 1: 853–856.
[2] Taghinezhad J, Mahmoodi E, Masdari M, Alimardani R. Spectral Analyses of an Optimized Ducted Wind Turbine using Hot-Wire Anemometry. 7th Iran Wind Energy Conference (IWEC2021) 2021: 1–4.
[3] Yin Y, Liao M, Lyu P. The dynamic stability analysis of wind turbines under different control strategies. 2015 5th International Conference on Electric Utility Deregulation and Restructuring and Power Technologies (DRPT) 2015: 2581–2586.
[4] Shi G, Zhang J, Cai X, Zhu M. Decoupling control of series-connected DC wind turbines with energy storage system for offshore DC wind farm. 2016 IEEE 7th International Symposium on Power Electronics for Distributed Generation Systems (PEDG) 2016: 1–6.
[5] Li Y, Zheng Y, Zhu N, Zhao F. Wind Turbine Kinetic Energy Accumulation and Release Regulation for Wind Farm Optimization. 2019 4th International Conference on Mechanical, Control and Computer Engineering (ICMCCE) 2019: 231–235.
[6] M. Cheng, Y. Zhu, The state of the art of wind energy conversion systems and technologies, Energy Convers Manag. 88 (2014) 332–347.
[7] V. Yaramasu, B. Wu, Basics of wind energy conversion systems (WECS). Model Predictive Control of Wind Energy Conversion Systems, John Wiley & Sons, 2016, pp. 1–467.
[8] M. Karabacak, H. Eskikurt, Design, modelling and simulation of a new nonlinear and full adaptive backstepping speed tracking controller for uncertain PMSM, Appl. Math. Model 36 (11) (2012) 5199–5213.
[9] H.W. Kim, M.J. Youn, K.Y. Cho, H.S. Kim, Nonlinearity estimation and compensation of PWM VSI for PMSM under resistance and flux linkage uncertainty, IEEE Trans. Control Syst. Technol. 14 (4) (2006) 589–601.
[10] J. Yang, W.H. Chen, S. Li, L. Guo, Y. Yan, Disturbance/Uncertainty Estimation and Attenuation Techniques in PMSM Drives, IEEE Trans. Ind. Electron. 64 (4) (2017) 3273–3285.
[11] T. Ishikawa, N. Igarashi, N. Kurita, Failure Diagnosis for Demagnetization in Interior Permanent Magnet Synchronous Motors, Int. J. Rotating Mach. 2 (2017) 716–814.
[12] T.D. Do, Disturbance observer-based fuzzy SMC of WECSs without wind speed measurement, IEEE Access 5 (2016) 147–155.
[13] H. Fathabadi, Novel maximum electrical and mechanical power tracking controllers for wind energy conversion systems, IEEE J. Emerg. Sel. Top. Power Electron. 5 (4) (2017) 1739–1745.
[14] A. Meza, Analysis of fuzzy observability property for a class of TS fuzzy models, IEEE Latin Am. Trans. 15 (4) (2017) 595–602.
[15] W.H. Chen, Nonlinear disturbance observer-enhanced dynamic inversion control of missiles, J. Guid., Control, Dyn. 26 (1) (2003) 161–166.
[16] K. Eom, I. Suh, W. Chung, Disturbance observer based path tracking control of robot manipulator considering torque saturation, Mechatronics 11 (2001) 325–343.
[17] T. Umeno, T. Kaneko, Y. Hori, Robust servosystem design with two degrees of freedom and its application to novel motion control of robot manipulators, IEEE Trans. Ind. Electron. 40 (5) (1993) 473–485.
[18] J. Ishikawa, M. Tomizuka, Pivot friction compensation using an accelerometer and a disturbance observer for hard disk drives, IEEE/ASME Trans. Mechatronics 3 (3) (1998) 194–201.
[19] B. Guvenc, L. Guvenc, Robust two degree-of-freedom add-on controller design for automatic steering, IEEE Trans. Control Syst. Technol. 10 (1) (2002) 137–148.
[20] Jd.J. Rubio, Hybrid controller with observer for the estimation and rejection of disturbances, ISA Trans. 65 (2016) 445–455.
[21] Jd.J. Rubio, G. Ochoa, R. Balcazar, J. Pacheco, Uniform stable observer for the disturbance estimation in two renewable energy systems, ISA Trans. 58 (2015) 155–164.
[22] W.H. Chen, A nonlinear disturbance observer for robotic manipulators, IEEE Trans. Industr. Electron. 47 (4) (2000) 932–938.
[23] A.M. Shotorbani, B. Mohammadi-Ivatloo, L. Wang, M. Marzband, M. Sabahi, Application of finite-time control Lyapunov function in low-power PMSG wind energy conversion systems for sensorless MPPT, Int. J. Electr. Power Energy Syst. 106 (2019) 169–182.
[24] M. Mansouri, M. Bey, S. Hassaine, M. Larbi, T. Allaoui, M. Denai, Genetic algorithm optimized robust nonlinear observer for a wind turbine system based on permanent magnet synchronous generator, ISA Trans. (2022).
[25] H.T. Nguyen, A.S. Al-Sumaiti, V.P. Vu, A. Al-Durra, T.D. Do, Optimal power tracking of PMSG based wind energy conversion systems by constrained direct control with fast convergence rates, Int. J. Electr. Power Energy Syst. 118 (2020) 105807.
[26] J. Chen, W. Yao, C.K. Zhang, Y. Ren, L. Jiang, Design of robust MPPT controller for grid-connected PMSG-Based wind turbine via perturbation observation based nonlinear adaptive control, Renewable Energy 134 (2019) 478–495.
[27] A. Dali, S. Abdelmalek, A. Bakdi, M. Bettayeb, A new robust control scheme: Application for MPP tracking of a PMSG-based variable-speed wind turbine, Renewable Energy 172 (2021) 1021–1034.
[28] A. Watil, A. El Magri, A. Raihani, R. Lajouad, F. Giri, An adaptive nonlinear observer for sensorless wind energy conversion system with PMSG, Control Eng. Practice 98 (2020) 104356.
[29] S. Das, B. Subudhi, A two-degree-of-freedom internal model-based active disturbance rejection controller for a wind energy conversion system, IEEE J. Emerg. Selected Top. Power Electron. 8 (3) (2019) 2664–2671.
[30] F. Bakhtiari, J. Nazarzadeh, Optimal estimation and tracking control for variable-speed wind turbine with PMSG, J. Modern Power Syst. Clean Energy 8 (1) (2019) 159–167.
[31] S. Li, M. Cao, J. Li, J. Cao, Z. Lin, Sensorless-based active disturbance rejection control for a wind energy conversion system with permanent magnet synchronous generator, IEEE Access 7 (2019) 122663–122674.
[32] Chen WH. Nonlinear Disturbance Observer Based Control for Nonlinear Systems with Harmonic Disturbances. 5th IFAC Sympos. on Nonlinear Control Systems 2001 2001; 34(6): 329– 334.

[33] A. Le, T.D. Do, High-order observers-based LQ control scheme for wind speed and uncertainties estimation in WECSs, Optim. Control Appl. Methods 39 (5) (2018) 1818–1832.
[34] Z. Zhang, Z. Li, M. Kazmierkowski, J. Rodrguez, R. Kennel, Robust predictive control of three-level NPC back-to-back power converter PMSG wind turbine systems with revised predictions, IEEE Trans. Power Electron. 33 (11) (2018) 9588–9598.
[35] R. Errouissi, A. Al-Durra, M. Debouza, A novel design of PI current controller for PMSG-based wind turbine considering transient performance specifications and control saturation, IEEE Trans. Ind. Electron. 65 (11) (2018) 8624–8634.
[36] A. Merabet, K. Ahmed, H. Ibrahim, R. Beguenane, Implementation of sliding mode control system for generator and grid sides control of wind energy conversion system, IEEE Trans. Sustain. Energy 7 (3) (2016) 1327–1335.
[37] K. Suleimenov, B. Sarsembayev, B. Phuc, T.D. Do, Disturbance Observer based Integral Sliding Mode Control for Wind Energy Conversion Systems, Wind Energy (2020) 1–22.
[38] L. Tan, T. Cong, D. Cong, Neural Network Observers and Sensorless Robust Optimal Control for Partially Unknown PMSM With Disturbances and Saturating Voltages, IEEE Trans. Power Electron. 36 (10) (2021) 12045–12056.
[39] D. Aziz, B. Jamal, Z. Othmane, M. Khalid, B. Bossoufi, et al., Implementation and validation of backstepping control for PMSG wind turbine using dSPACE controller board, Energy Reports 5 (2019) 807–821.
[40] T.D. Do, H.T. Nguyen, A Generalized Observer for Estimating Fast–Varying Disturbances, IEEE Access 6 (2018) 28054–28063.
[41] L. Pan, C. Shao, Wind energy conversion systems analysis of PMSG on offshore wind turbine using improved SMC and Extended State Observer, Renewable Energy 161 (2020) 149–161.
[42] X. Yu, O. Kaynak, Sliding-mode control with soft computing: A survey, IEEE Trans. Ind. Electron. 56 (9) (2009) 3275–3285.
[43] D. Murray-Smith, Modelling and Simulation of Integrated Systems in Engineering, Woodhead Publishing, Sawston, Cambridge, 2012.
[44] A. Anufriev, Y. Makarichev, Y. Zubkov, V. Pevchev, Mathematical model of a synchronous generator of a low-power wind power plant, 3, Bulletin of the Samara State Technical University. Series Technical Sciences, 2017, pp. 66–74.
[45] O. Aguilar, R. Tapia, A. Valderrabano, H. Minor, Design and performance comparison of pi and adaptive current controllers for a WECS, IEEE Lat. Am. Trans. 13 (5) (2015) 1361–1368.
[46] E. Kim, F. Mwasilu, H. Choi, J. Jung, An Observer-Based Optimal Voltage Control Scheme for Three-Phase UPS Systems, IEEE Trans. Industr. Electron. 62 (4) (2015) 2073–2081.
[47] M.J. Corless, G. Leitmann, Continuous state feedback guaranteeing uniform ultimate boundedness for uncertain dynamic systems, IEEE Trans. Autom. Control 26 (1981) 1139–1144.
[48] K.S. Kim, K.H. Rew, S. Kim, Disturbance Observer for Estimating Higher Order Disturbances in Time Series Expansion, IEEE Trans. Autom. Control 55 (8) (2010) 1905–1911. doi: 10.1109/TAC.2010.2049522.
[49] F. Valenciaga, P.F. Puleston, High-Order Sliding Control for a Wind Energy Conversion System Based on a Permanent Magnet Synchronous Generator, IEEE Trans. Energy Convers. 23 (3) (2008) 860–867. doi: 10.1109/TEC.2008.922013.
[50] A.V. Le, T.D. Do, High-order observers-based LQ control scheme for wind speed and uncertainties estimation in WECSs, Optimal Control Appl. Methods 39 (5) (2018) 1818–1832.
[51] K. Liu, Z. Zhu, J. Zhang, Q. Zhang, A. Shen, Multi-parameter estimation of non-salient pole permanent magnet synchronous machines by using evolutionary algorithms, IEEE (2010) 766–774.
[52] K. Liu, Q. Zhang, J. Chen, Z.Q. Zhu, J. Zhang, Online multiparameter estimation of nonsalient-pole PM synchronous machines with temperature variation tracking, IEEE Trans. Industr. Electron. 58 (5) (2010) 1776–1788.

Altynay Kashaganova received the B.S. degree in engineering and technology from Department of Radio Engineering, Electronics and Telecommunications, Faculty of Physics and Technology, L.N. Gumilyov Eurasian National University, Astana, Kazakhstan, in 2014, where she received the M.S. degree of technical sciences from Department of Nanomaterials and Nanotechnologies, Faculty of Physics and Technology, in 2016, and the Ph. D. candidate degree with the Department of System Analysis and Control, Faculty of Information Technology. Her current research interests include control of electric machine drives used in wind energy conversion systems.

Kanat Suleimenov received the B.S. degree in engineering and technology from Kazakh-British Technical University, Almaty, Kazakhstan, in 2014, and the M.S. degree in mechanical engineering from Nazarbayev University, Nur-Sultan, Kazakhstan, in 2019, where he is currently pursuing the Ph.D. degree with the Department of Robotics and Mechatronics. From November 2014 to August 2015, he was with Coca-Cola Almaty Bottlers Company, where he served as an Operator on the production line. From 2016 to 2017, he worked as a Laboratory Technician with the Department of Mechanical Engineering, School of Engineering, Nazarbayev University. From February 2018 to August 2019, he worked as a Research Assistant in the Power Conversion and Motion Control Laboratory, under the supervision of Dr. Ton Duc Do. His current research interests include control of electric machine drives used in electric cars and wind energy conversion systems.

Saule Sagnaeva photograph and biography are not available at the time of publication.

Ton Duc Do (Senior Member, IEEE) received the B.S. and M.S. degrees in electrical engineering from the Hanoi University of Science and Technology, Hanoi, Vietnam, in 2007 and 2009, respectively, and the Ph.D. degree in electrical engineering from Dongguk University, Seoul, South Korea, in 2014. From 2008 to 2009, he worked at the Division of Electrical Engineering, Thuy Loi University, Vietnam, as a Lecturer. He was at the Division of Electronics and Electrical Engineering, Dongguk University, as a Postdoctoral Researcher, in 2014. He was also a Senior Researcher at the Pioneer Research Center for Controlling Dementia by Converging Technology, Gyeongsang National University, South Korea, from May 2014 to August 2015. Since September 2015, he has been an Assistant Professor and then Associate Professor with the Department of Robotics and Mechatronics, Nazarbayev University, Kazakhstan. His research interests include the field of advanced control system theories, electric machine drives, renewable energy conversion systems, uninterruptible power supplies, electromagnetic actuator systems, targeted drug delivery systems, and nanorobots. He has been an Associate Editor of IEEE ACCESS since April 2017. He has been aslo a Guest Editor for special issues of several journals such as Mathematical Problems in Engineering, Electronics, Sensors. He received the Best Research Award from Dongguk University in 2014, Most Cited Paper Award from Wind Energy in 2020–2021, and Outstanding Associate Editor of IEEE ACCESS in 2021. He was recently listed in the most influenced scientists with both single year and career-wide tables based on a systematic bibliometric study by researchers from Stanford University, published on November 3, 2022.